Chapter 2
Mean Field Theory of Slip Statistics

Karin A. Dahmen

Abstract A simple mean field model for the statistics and the dynamics of slip avalanches in slowly deformed solids is reviewed. Its universal scaling predictions are compared to experiments on slowly compressed single nanocrystals, microcrystals, bulk metallic glasses, and rocks, as well as to slowly sheared jammed granular materials, and to earthquakes. The remarkable agreement between model and experiments spanning 12 decades in length and a wide range of material structures implies that results on the slip statistics can be transferred from one solid material to another and from one scale to another. Potential applications of the results include materials testing, failure prediction, and hazard prevention.

2.1 Introduction

Slowly sheared crystals, bulk metallic glasses, composite materials, ferroelastic materials, densely packed granular materials, rocks, and the earth's crust all deform in a jerky way via (slip-) avalanches, such as earthquakes. These slip avalanches have a broad distribution $D(S)$ of sizes S, following simple functions that are independent of the microscopic details of the material. Recent experiments, analytic models, and simulations show that the avalanche size distribution typically follows a power law over a broad range of sizes, similar to the Gutenberg Richter law of earthquakes. The power law region is cut off at a size $S = S_{max}$ that may depend on the applied stress, strainrate, temperature, or sample size [1–5].

A simple mean field model [5] has proven useful not only for gaining an intuition for these slip avalanches (also called "serrations" of the stress strain curves), but also for organizing the experimental data. The model also predicts the observed statistics of the avalanches, the avalanche dynamics, the time series properties

K.A. Dahmen (✉)
Department of Physics, University of Illinois at Urbana-Champaign,
Urbana, IL 61801, USA
e-mail: dahmen@illinois.edu

E.K.H. Salje et al. (eds.), *Avalanches in Functional Materials and Geophysics*,
Understanding Complex Systems, DOI 10.1007/978-3-319-45612-6_2

of the avalanches, and their dependence on the experimental tuning parameters [1–4, 6, 11]. In the following we briefly review the model, its predictions, and its comparison to first experiments.

2.2 The Model

The model assumes that a solid material has weak spots [5]. As the material is slowly sheared the local shear stress increases everywhere. Each weak spot is stuck until the local shear stress exceeds its random failure threshold. When that happens it slips by a random amount, and the released stress is redistributed to the other weak spots. This may trigger some of the other weak spots to slip also, leading to a failure cascade, or slip avalanche. The avalanche stops when everywhere in the material the local stress is below its respective local failure threshold.

After an avalanche is completed, the applied stress is slowly increased further until the next weak spot slips, thereby triggering the next slip avalanche. The model can be written [5] either in a continuum description or a discrete description. Both are reviewed below.

2.2.1 Continuum Version of the Model

One can write the following equation of motion for the model [5, 8]:

$$\eta \quad \partial \mathrm{u}(\mathbf{r},\mathrm{t})/\partial \mathrm{t} = \mathrm{F} + \sigma_{\mathrm{int}}(\mathbf{r},\mathrm{t}) - \mathrm{f_R}[\mathrm{u},\mathbf{r},\{(\mathrm{u}(\mathbf{r},\mathrm{t}' < \mathrm{t})\}] \tag{2.1}$$

where η is a damping constant, F is the applied shear stress in the x direction (using scalar elasticity). $u(\boldsymbol{r}, t)$, is the accumulated slip in the x direction at point $\boldsymbol{r}$ and at time t (e.g. the displacement discontinuity across the slip plane or shear band, or earthquake fault), and

$$\sigma_{\mathrm{int}}(\mathbf{r},\mathrm{t}) = \int_{-\infty}^{\mathrm{t}} \mathrm{dt}' \int \mathrm{d}^2\mathrm{r}' \quad \mathrm{J}(\mathbf{r}-\mathbf{r}', \mathrm{t}-\mathrm{t}') \times [\mathrm{u}(\mathbf{r}', \mathrm{t}') - \mathrm{u}(\mathbf{r},\mathrm{t})] \tag{2.2}$$

is the shear stress accumulated at point $\boldsymbol{r}$, at time t, resulting from elastic stress transfer from all previous slips in the solid since time $t = 0$ when the system started in a relaxed state. f_R represents the quenched random "pinning" stress, that prevents slips until the local stress exceeds the local failure threshold, as discussed above. This failure threshold may be history dependent (see also the discussion of the discrete version of the model below). A renormalization group analysis of the model for positive couplings shows that the coupling between slips of weak spots is sufficiently long range (for example, $\mathrm{J}(\mathbf{r}) \equiv \int \mathrm{dt}\, \mathrm{J}(\mathbf{r},\mathrm{t}) \sim \mathrm{r}^{-2}$ for parallel straight edge

dislocations) that mean field theory (MFT) gives the correct scaling behavior in all dimensions [5, 8]. For small patches slipping along a fault-like plane surrounded by elastic material $J(\mathbf{r}) \equiv \int dt\, J(\mathbf{r}, t) \sim r^{-3}$ and mean field theory is expected to apply for 2 and higher dimensional slip planes [5, 8]. In most solids the slips or slip avalanches organize predominantly along shear bands or glide planes, and the positivity of the coupling applies during avalanches [8–10]. In fact the predictions of MFT agree with the scaling behavior of the avalanche statistics seen in experiments on crystals, bulk metallic glasses, high entropy alloys, rocks, granular materials, and earthquakes [1–3, 6, 11].

2.2.2 Discrete Version of the Model

A simple discrete version of the model can be easily solved in mean field theory.

For a block of material two different loading conditions may be applied:

(I) a slowly increasing shear stress F applied to the boundaries
(II) a small strain rate imposed at the boundaries.

The model predicts that the scaling behavior for both boundary conditions is the same, as was recently also confirmed by experiments [32].

In the discrete version the material is modeled by N lattice points marked by $l=1,\ldots,N$. Each lattice point (or weak spot) has its own random *local* failure shear stress $\tau_{s,l}$. We assume it deforms elastically until the local shear stress exceeds this local threshold. When that happens, the weak spot slips until the local shear stress is reduced to a lower arrest stress $\tau_{a,l}$("sticking stress"). $\tau_{s,l}$ and $\tau_{a,l}$ vary randomly in space, to model the disorder in the material. After re-sticking the weak spot locally acts again elastically until the local stress again exceeds the failure stress.

Brittle materials: To model brittle (or hardening) materials, the failure stress is assumed to weaken (or strengthen, respectively) after the initial slip in an avalanche. For brittle materials, after a point l slips for the first time during an avalanche, the local failure threshold is weakened from the static value $\tau_{s,l}$ to a diminished value $\tau_{d,l}$ with $\tau_{a,l} < \tau_{d,l} < \tau_{s,l}$. The failure stress remains at $\tau_{d,l}$ until the avalanche has been completed. The amount of weakening is given by the weakening parameter $\varepsilon = (\tau_{s,l} - \tau_{d,l})/\tau_{s,l}$ [5, 8]. After the completion of an avalanche all weakened failure stresses are reset to their initial static values $\tau_{s,l}$.

Hardening Materials: In contrast, for hardening materials upon slipping the failure thresholds are strengthened by an amount proportional to $\varepsilon < 0$, to model the local energy absorption due to dislocation pair creation and entanglement etc. [4, 5].

Avalanches: The stress that is released during a slip is redistributed to all other cells in MFT. In MFT the coupling is replaced by a function that is constant in space: $J(\mathbf{r}) \equiv J/N$. The coupling causes slip avalanches. The local stress τ_l at a lattice point l is given by $\tau_l = J/N \Sigma_m (u_m - u_l) + F$ [5], where F is the applied stress and u_l is the local displacement discontinuity. As described above, each point fails when

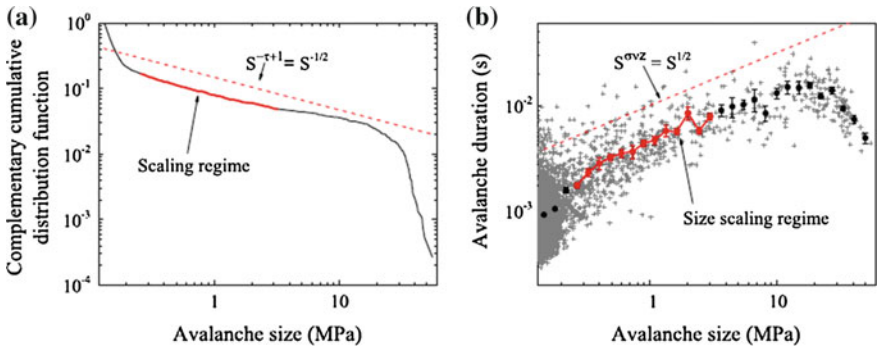

Fig. 2.1 Figures reprinted from [6]. Avalanche statistics for quasistatic uniaxial compression of two specimens of $Zr_{45}Hf_{12}Nb_5Cu_{15.4}Ni_{12.6}Al_{10}$. The predictions of the mean field model are shown by the *dashed red lines*. The data in the scaling regime are also highlighted in *red*. **a** The distribution of stress drop sizes for the 3744 avalanches; the data in the scaling regime have the expected mean field exponent of –1/2. **b** The avalanche duration as a function of avalanche size. The data in the scaling regime have the expected mean field exponent of 1/2

the local stress is bigger than the local failure threshold (slip stress) $\tau_{f,l} \equiv \tau_{s,l}$ (or $\tau_{d,l}$). When site l fails, it slips by an amount Δu_l resulting in a stress reduction $\tau_{f,l} - \tau_{a,l} \sim 2G\Delta u_l$ where $G \sim J$ is the elastic shear modulus. After a slip the site resticks and the released stress is redistributed to the other sites in the system. A local slip can then trigger other sites to slip in a slip-avalanche. The avalanche ends when at all sites the local stresses are below their local failure stresses $\tau_l < \tau_{f,l}$. In the adiabatic (slow driving) limit, the applied stress F is increased only after a slip avalanche has been completed, until the next site fails. For small applied strain rate Ω the stress F in the dynamical equation is replaced by $K_L(\Omega t - u_i)$ where K_L is an effective loading spring constant [5, 8], which is proportional to $G/N^{(1/2)}$.

This model can be solved analytically [5, 8]. It predicts the observed scaling behavior of the slip statistics without the need for any fitting parameters or any assumptions about length scales or material structures. As a result, it predicts the same slip statistics for a wide range of scales and materials (Fig. 2.1) [1, 5]. The key model parameters are: the weakening ε, the boundary conditions, $\tau_{s,r}, \tau_{a,r}$ and their distributions, the values of η and the elastic constants, and the form of $J(\boldsymbol{r}, t) > 0$. Among these, only ε, and the range of $J(\boldsymbol{r}, t)$ affect the universal (i.e. detail independent) aspects of the behavior on long length scales.

2.2.2.1 Model Predictions for Avalanche Statistics and Comparison to Experiments

For zero weakening (ε=0) the model predicts the scaling behavior of the slip statistics on long length scales for a wide range of materials, irrespective of the microscopic details. In particular it predicts the probability distributions of $D(S)$ of finding

avalanches of size S at applied shear stress F [5, 8]:

$$D(S, F) \sim 1/S^{\kappa} G_S(S(F - F_c)^{1/\sigma}) \quad \text{where in MFT } \kappa = 1.5 \text{ and } 1/\sigma = 2$$
$$\text{and } G_S(x) \sim A' exp(-B'x),$$

with A' and B' non-universal constants. F_c is the flow stress or critical stress. The avalanche size S could be the total slip for experiments with slowly increasing applied shear stress, or total stress drop for experiments at imposed slow strain rate. Similarly it predicts the probability of finding avalanches of energy E at stress $F$to scale as [12].

$D(E, F)$. $\sim 1/E^{-\eta} G_E(E(F_c - F)^{(2-\sigma \upsilon z)/\sigma})$ with η=*4/3* and $(2-\sigma \upsilon z)/\sigma = 3$, $\sigma \upsilon z = 0.5, \sigma = 0.5$ and $G_E(x)$ is another universal scaling function [3, 13]. Here the energy E scales as $E \sim \int v^2(t)\, dt$, and $v(t)$ is proportional to the instantaneous growth rate of the avalanche (either the slip rate for slowly increasing stress or the stress drop rate for slow strain rate boundary conditions). In some experiments histograms of avalanche energies or sizes are collected over the entire stress range, in that case $D(S, F)$ and $D(E, F)$are integrated over the applied stress F, from 0 to F_c, which yields the power law stress-integrated histograms $D_{int}(S) \sim S^{-(\kappa+\sigma)}\ G_{int,S}\,(S/S_{max})$. Here $S_{max}$is a measure for the largest observed avalanche size, which is usually a function of the tuning parameters in the system, such as temperature, sample size, etc. $G_{int,S}(x)$ is another scaling function. In some acoustic emission experiments the energy may be defined as $E_m \sim (v(t))^2_{max}$ i.e. as proportional to the highest slip-velocity squared during an avalanche [1]. In MFT histograms of this quantity scale as $D(E_m, F) \sim (E_m)^{-(\mu+1)/2}\ G_{Em}(E_m/E_{m,max})with E_{m,max} \sim (F_c - F)^{-2\rho}$ where $(\mu + 1)/2 = 1.5$ and $2\rho = 2$ in MFT and $G_{Em}(x)$ is yet another scaling function. Correspondingly the stress integrated distribution scales as $D_{int}(E_m) \sim (E_m)^{-[(\mu+1)/2+1/(2\rho)]}$ $G_{int,Em}(E_m/E_{m,max})) \sim (E_m)^{-2}\ G_{int,Em}(E_m/Em_{,max})$ [14, 15]. Table 2.1 summarizes some of the results from MFT. All symbols with a subscript "max" (or "min") denote maximum (or minimum) values of the scaling variable, that typically depend on experimental tuning parameters, such as temperature, sample size, and others. The results shown in Table 2.1 are compiled from references [1, 5, 12, 14, 15]. Table 2.1a, b show some of the scaling relations predicted by mean field theory, while Table 2.1c shows the comparison to a wide range of recent experiments. A comparison of some of these predictions to experiments on the slow shear of nanocrystals, amorphous materials, rocks, granular materials, and the earth's crust is shown in [1].

The most extensive comparison to experiments has probably been done for bulk metallic glasses (BMGs), which shows agreement with the model predictions for more than 12 different statistical quantities [6]. For BMGs that are compressed at slow strainrate, Fig. 2.1 shows the complementary cumulative stress drop size distribution $C(S) = \int_S^{\infty} D\left(S'\right) dS'$ which gives the probability to observe avalanches larger than size S. For deformation in the steady state, the mean field model

Table 2.1 Results form MFT

Statistical Distributions	**Scaling forms predicted by the model** *[5-7]*
D(S,F), of avalanche size, *S* (slip size or stress drop at stress *F*)	$D(S) \sim S^{-\kappa}\, G_S(S/S_{max})$
$D_{int}(S)$ of avalanche size S integrated over stress *F*	$D_{int}(S) \sim S^{-(\kappa+\sigma)}\, G_{int,S}(S/S_{max})$
D(v,F), of stress-drop rate, *v*	$D(v) \sim v^{-\psi}\, G_V(v/v_{max})$
D(T,F), of avalanche durations, *T*	$D(T) \sim T^{-\alpha} G_T(T/T_{max})$
$D_{int}(T)$ of avalanche durations integrated over stress F	$D_{int}(T) \sim T^{(\alpha+1/(\nu z))}\, G_{int,T}(T/T_{max})$
Power spectrum of the stress drop rate versus time, *P(ω,F),* at frequency, *ω*	$P(\omega) \sim \omega^{-(1/\sigma\nu z)} D_\omega(\omega/\omega_{min})$
D(E,F), of energy $E \sim \int v^2 dt$ released in a slip close to failure	$D(E,F) \sim E^{-\eta}\, G_E(E/E_{max})$
$D_{int}(E)$ of energy $E \sim \int v^2 dt$ integrated over stress *F*	$D_{int}(E) \sim E^{-(\eta+\sigma/(2-\sigma\nu z))}\, G_{int,E}(E/E_{max})$
$D(E_m, F)$ of peak velocity squared $E_m \sim v^2_{max}$	$D(E_m,F) \sim (E_m)^{-(\mu+1)/2} G_{Em}(E_m/E_{m,max})$
$D_{int}(E_m)$ of peak velocity squared $E_m \sim v^2_{max}$ integrated over stress *F*	$D_{int}(E_m) \sim (E_m)^{-[(\mu+1)/2+1/(2\rho)]} G_{int,Em}(E_m/E_{m,max})$
$D(v_m,F)$ of maximum velocities v_m during avalanche	$D(v_m,F) \sim (v_m)^{-\mu} G_{vm}(v_m/v_{m,max})$
$D_{int}(v_m)$ of max. velocities v_m integrated over stress *F*	$D_{int}(v_m) \sim (v_m)^{-(\mu+1/\rho)}\, G_{int,vm}(v_m/v_{m,max})$

(a)

Scaling relations	**Exponent values in Mean Field Theory (MFT)**	**Exponent relations**
$\langle E \mid S \rangle \sim S^2/\langle T \mid S \rangle \sim S^{2-\sigma\nu z}$	$2-\sigma\nu z=3/2$	$(\kappa-1)=(\eta-1)(2-\sigma\nu z)$, $\eta=4/3$ in MFT
$\langle S \mid T \rangle \sim T^{(1/\sigma\nu z)}$	$1/(\sigma\nu z)=2$	$\kappa_{int} \equiv \kappa+\sigma=2$ (in MFT for the stress integrated exponent of $D_{int}(S)$)
$\langle T \mid S \rangle \sim S^{\sigma\nu z}$	$\sigma\nu z=1/2$	$\eta_{int} \equiv \eta + \sigma/(2-\sigma\nu z)=5/3$ (in MFT for stress integrated exponent of $D_{int}(E)$)
$\langle v_m \mid S \rangle \sim S^{\sigma\rho}$	$\rho\sigma=1/2$	$(\kappa_{int}-1) = (\eta_{int}-1)(2-\sigma\nu z)$
$\langle v_m \mid T \rangle \sim T^{(\rho/(\nu z))}$	$\rho/(\nu z)=1$	
$\langle E \mid S \rangle \sim S^{2-\sigma\nu z}$	$2-\sigma\nu z=3/2$	
$\langle E_m \mid S \rangle \sim S^{2\sigma\rho}$	$2\sigma\rho=1$	
$\langle E \mid T \rangle \sim T^{(2-\sigma\nu z)/(\sigma\nu z)}$	$(2-\sigma\nu z)/(\sigma\nu z)=3$	$(\kappa-1)=(\alpha-1)\sigma\nu z$
$\langle E_m \mid T \rangle \sim T^{2\rho/(\nu z)}$	$2\rho/(\nu z)=2$	
Strain-rate $\langle v \mid F \rangle \sim (F-F_c)^{\beta}$ for $F > F_c$ (depinned)	$\beta=1$	

Fixed-stress loading conditions: slowly increasing stress, *F*, up to the failure stress, F_c	**Fixed-strain-rate loading conditions: moving the boundary at a slow strain rate, *Ω***
$S_{max} \sim (F_c-F)^{-1/\sigma}$	$S_{max} \sim \Omega^{-\lambda/(\sigma z\nu)}$
$v_{max} \sim (F_c-F)^{-1}$	$v_{max} \sim \Omega^{-1}$
$T_{max} \sim (F_c-F)^{-\nu z}$	$T_{max} \sim \Omega^{-\lambda}$
$\omega_{min} \sim (F_c-F)^{\nu z}$	$\omega_{min} \sim \Omega^{\lambda}$
$E_{max} \sim (F_c-F)^{-(2-\sigma\nu z)/\sigma}$	$E_{max} \sim \Omega^{-(2-\sigma\nu z)\lambda/(\sigma\nu z)}$
$E_{m,max} \sim (F_c-F)^{-2\rho}$	$E_{m,max} \sim \Omega^{-2\rho\lambda/(\nu z)}$
$v_{m,max} \sim (F_c-F)^{-\rho}$	$v_{m,max} \sim \Omega^{-\rho\lambda/(\nu z)}$

(b)

(continued)

Table 2.1 (continued)

Exponents	Sample Size	κ	$\kappa_{int}=\kappa+\sigma$	σ	$1/\sigma\nu z$	α	ψ	$\lambda\equiv\nu z/\beta$	η	μ	ρ	β
Model Predictions												
Mean Field Theory (MFT) [5,14,15]		**1.5**	2	0.5	2	2	1	1	4/3	2	1	1
Experimental Verifications*												
Nanocrystals (Molybdenum (Mo), Compression, see [3,16]	10^{-8} m	**1.5**	2	0.5	2							
Microcrystals (Nickel (Ni), Compression [4,17])	10^{-6} m	**1.5**			2							
Bulk Metallic Glass (BMG) ($Cu_{47}Zr_{47.5}Al_5$ [18], $Zr_{45}Hf_{12}Nb_5Cu_{15.4}Ni_{12.6}Al_{10}$ [6], and $Zr_{64.13}Cu_{15.75}Ni_{10.12}Al_{10}$ [2], atomic percent) Compression.	10^{-3} m	**1.5**	2	0.5	2	2						
Lab-scale rocks (Sidobre granite, Compression [19,20,21])	10^{-2} m	**~1.5**	1.66-2.2									
Lab-scale rocks (Westerly granite, Frictional sliding [22])	10^{-2} m	**~1.5**										
Jammed granular materials (Photo-elastic disks in Couette cells and other geometries also in 3 dimensions [23,24])	1 m	**~1.5**			1.8-2.5	~2						
Earthquakes [25,26,27]	10^{5} m	**~1.5**			2							

(c)

(continued)

Table 2.1 (continued)

Lab-scale rocks (Sidobre granite, Compression [19,20,21])	10^{-2} m	**~1.5**	1.66-2.2									
Lab-scale rocks (Westerly granite, Frictional sliding [22])	10^{-2} m	**~1.5**										
Jammed granular materials (Photo-elastic disks in Couette cells and other geometries [23])	1 m	**~1.5**			1.8-2.5	~2						
Earthquakes [25,26,27]	10^{5} m	**~1.5**			2							

(c)

**Exponents from experiments and observations quoted here have a 10% error range due to statistical fluctuations* [1]. *Exponents from previous rock experiments were obtained from* [19, 20] *at the largest stresses, using that the Gutenberg Richter exponent, b, in* [19] *is related to our exponents via b = 3(κ-1)/2 (see* [8, 21]*). For the relationship between the slip-size and the acoustic-emission signal see* [21]*, the Supplementary Information of* [3, 15]*, and references therein*

predicts $C(S) \sim S^{-(\kappa-1)}$ for a certain scaling regime range of (small) avalanche sizes $S_{min} < S < S_{max}$, with $\kappa = 1.5$. Power laws fitted to experimental data on crystals and bulk metallic glasses are consistent with mean field theory $\kappa - 1 = 0.51 \pm 0.03$ [3, 5, 6, 19]. For models of brittle materials, such as BMGs, the weakening parameter $\varepsilon > 0$ and the model predicts additional large (i.e. system spanning) avalanches that recur almost periodically, with the power law distributed smaller avalanches observed in between the occurrence of the large avalanches [5, 6, 23]. Both small and large avalanches have recently been observed in experiments on BMGs [6, 7].

2.3 Model Predictions for Avalanche Dynamics and Comparison to Experiments

The MFT model also predicts average temporal profiles of the avalanches, The time profile for the average stress drop rate $< -d\sigma/dt(t)|T >$, which is obtained by averaging the stress drop rate $-d\sigma/dt(t) > 0$ over all avalanches of the same duration T, is predicted by mean field theory to follow a parabola. (An avalanche starts when $-d\sigma/dt(t)$ first becomes positive and it stops when it becomes negative again.). The predictions for the scaling behavior of these profiles have recently been tested for

bulk metallic glasses for the first time [6]. Machine stiffness effects can flatten out the shape [6]. An asymmetric profile, i.e. one that is tilted to the right or to the left, can be an indication that either inertia or delay effects play an important role in the slip dynamics [5, 23, 28–31].

Also, the time profile for the average stress drop rate $< -d\sigma/dt(t)|S >$, which is obtained by averaging $-d\sigma/dt(t)$ over all avalanches of the same total stress drop size S, is predicted by MFT to follow a function of the form $< -d\sigma/dt(t)|S > \sim S^{1-\sigma\upsilon z} G'(t/S^{\sigma\upsilon z})$ with $\sigma\upsilon z = 0.5$ in MFT, and $G'(x) = A'x\exp(-B'x^2)$ where A' and B' are experiment-specific constants [1, 5, 6].

Examples of these shapes are shown in Fig. 2.2. References [2, 6] contain the comparison of many more statistical properties with the model predictions.

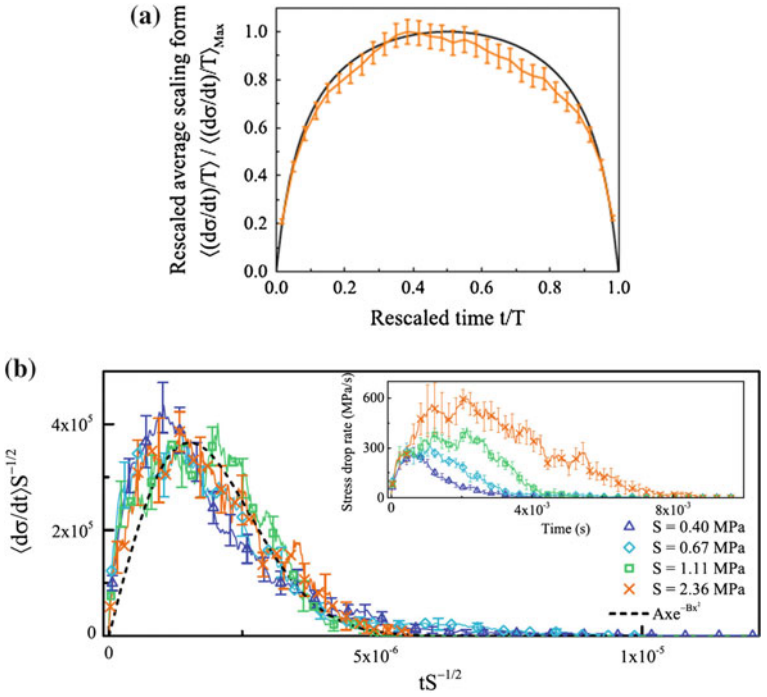

Fig. 2.2 Figures reprinted from [6]. **a** The average avalanche shape constructed from all avalanches in the scaling regime. The stress drop rate is scaled by the maximum stress drop rate for each avalanche on the vertical axis and by the avalanche duration on the horizontal time axis. The mean field prediction is also shown. **b** The unscaled shapes for several small avalanches of various sizes are shown in the *inset*. When both axes are scaled by $S^{-1/2}$, the shapes collapse to the form predicted by the mean field model (*black dashed line*). (From [6])

2.4 Conclusion

Initial measurements indicate that mean field theory makes many predictions for experiments, some of which have been tested for a range of materials. Initial comparisons of theory with experiments suggest that the universality class of the simple mean field model may be surprisingly large [1]. Table 2.1 shows that so far only a subset of the model predictions have been tested in experiments. More experimental tests, especially tests at high time resolution on a wide range of materials are needed to fully test all predictions of the model and to establish the size of the underlying universality class. Regardless of whether or not a material's slip statistics agree precisely with the predictions of the simple model for the scaling exponents and scaling functions, the model provides valuable intuition and guidance for organizing the data of experiments and simulations. As recent experiments show [1, 6], the model predictions agree with experiments on a surprisingly wide range of materials, including crystals, BMGs, rocks, granular materials, and earthquakes [1].The reason for this agreement of the simple mean field model with so many experiments likely lies in the fact that most experiments show some kind of slip localization so that the avalanches typically propagate in gilde planes, shear bands, or earthquake faults. For this kind of slip localization one can use tools from the theory of phase transitions, like the renormalization group, to show that the elastic interactions are positive along such shear bands and that the discussed mean field theory is expected to fully describe the scaling behavior on long length scales, in 3 dimensions (up to negligible logarithmic corrections) [8]. Experiments and simulations of other systems, such as ferroelastics also give related results [12, 33]. Potential applications of the model include materials testing, failure prediction and hazard prevention [34].

Acknowledgments We thank Michael LeBlanc, Ekhard Salje, Jonathan Uhl, and Wendelin Wright for key contributions to this short review article. This work was supported by the National Science Foundation under Grants CBET–1336634, and DOE DE-FE-0011194 (KAD). We especially thank the Kavli Institute for Theoretical Physics for hosting the author for a workshop during which parts of this paper were written and for support through grant NSF PHY11–25915.

References

1. J.T. Uhl, S. Pathak, D. Schorlemmer, X. Liu, R. Swindeman, B.A.W. Brinkman, M. LeBlanc, G. Tsekenis, N. Friedman, R. Behringer, D. Denisov, P. Schall, X. Gu, W.J. Wright, T. Hufnagel, A. Jennings, J.R. Greer, P.K. Liaw, T. Becker, G. Dresen, K.A. Dahmen, Universal quake statistics: from compressed nanocrystals to earthquakes. Sci. Reports **5**, 16493 (2015)
2. J. Antonaglia, X. Xie, M. Wraith, J. Qiao, Y. Zhang, P.K. Liaw, J.T. Uhl, K.A. Dahmen, Tuned critical avalanche scaling in bulk metallic glasses. Nature Sci. Reports **4**, 4382 (2014)
3. N. Friedman, A.T. Jennings, G. Tsekenis, J.-Y. Kim, J.T. Uhl, J.R. Greer, K.A. Dahmen, Statistics of dislocation slip-avalanches in nano-sized single crystals show tuned critical behavior predicted by a simple mean field model. Phys. Rev. Lett. **109**, 095507 (2012)
4. M. Zaiser, Scale invariance in plastic flow of crystalline solids. Adv. Phys. **55**, 185–245 (2006). (and references therein)

5. K.A. Dahmen, Y. Ben-Zion, J.T. Uhl, Micromechanical model for deformation in solids with universal predictions for stress strain curves and slip avalances. Phys. Rev. Lett. **102**, 175501 (2009)
6. J. Antonaglia , W.J. Wright, X.J. Gu, R.R. Byer, T.C. Hufnagel, M. LeBlanc M, J.T. Uhl, and K.A. Dahmen, Bulk Metallic Glasses Deform via Slip-avalanches. Phys. Rev. Lett. **112**, 155501/1–4 (2014)
7. W.J. Wright, Y. Liu, X. Gu, K.D. Van Ness, S.L. Robare, X. Liu, J. Antonaglia, M. LeBlanc, J.T. Uhl, T.C. Hufnagel, K.A. Dahmen, Experimental evidence for both progressive and simultaneous shear during quasistatic compression of a bulk metallic glass. J. Appl. Phys. **119**, 084908 (2016). doi:10.1063/1.4942004
8. D.S. Fisher, K.A. Dahmen, S. Ramanathan, Y. Ben-Zion, Statistics of earthquakes in simple models of heterogeneous faults. Phys. Rev. Lett. **78**, 4885–4888 (1997)
9. J.P. Sethna, Private communication
10. J.T. Uhl, Private communication
11. R. Carroll, C. Lee, C.-W. Tsai, J.-W. Yeh, J. Antonaglia, B. Brinkman, M. LeBlanc, X. Xie, S. Chen, P.K. Liaw, K.A. Dahmen, Experiments and model for serration statistics in low-entropy, medium-entropy, and high-entropy alloys. Sci. Reports **5**, 16997 (2015). doi:10.1038/srep16997
12. E.K.H. Salje, K.A. Dahmen, Crackling noise in disordered materials. Annu. Rev. Condens. Matter Phys. **5**, 233–254 (2014)
13. K. A. Dahmen, *Hysteresis, avalanches, and disorder-induced critical behavior: a renormalization group approach*. Ph.D. thesis, Cornell Univ., Ithaca, NY (1995) 233 pp
14. M. LeBlanc, L. Angheluta, K.A. Dahmen, N. Goldenfeld, Universal fluctuations and extreme statistics of avalanches near the depinning transition. Phys. Rev. E **87**, 022126 (2013)
15. M. LeBlanc, L. Angheluta, K. Dahmen, N. Goldenfeld, Distribution of maximum velocities in avalanches near the depinning transition. Phys. Rev. Lett. **109**, 105702 (2012)
16. S. Brinckmann, J.-Y. Kim, J.R. Greer, Fundamental differences in mechanical behavior between two types of crystals at nano-scale. Phys. Rev. Lett. **100**, 155502/1–4 (2008)
17. D. Dimiduk, C. Woodward, R. LeSar, M. Uchic, Scale-free intermittent flow in crystal plasticity. Science **312**, 1188–1190 (2006)
18. B.A. Sun et al., Plasticity of ductile metallic glasses: A self-organized critical state. Phys. Rev. Lett. **105**, 035501/1–4 (2010)
19. D. Amitrano, Brittle-ductile transition and associated seismicity: experimental and numerical studies and relationship with the *b*-value. Geophys. Res. **108**B1, 2044/1–15 (2003). doi:10.1029/2001JB000680
20. C.H. Scholz, The Frequency-magnitude relation of microfracturing in rock and its relation to earthquakes. Bull. Seismol. Soc. Am. **58**, 399–415 (1968)
21. D. Amitrano, Variability in the power-law distributions of rupture events. Eur. Phys. J. **205**, 199–215 (2012)
22. T.H.W. Goebel et al., Identifying fault heterogeneity through mapping spatial anomalies in acoustic emission statistics. J. Geophys. Res. **117**, B03310/1–18 (2012). doi:10.1029/2011JB008763
23. K.A. Dahmen, Y. Ben-Zion, J.T. Uhl, A simple analytic theory for the statistics of avalanches in sheared granular materials. Nat. Phys. **7**, 554–557 (2011)
24. D.V. Denisov, K.A. Lorincz, J.T. Uhl, K.A. Dahmen, P. Schall, Universality of slip avalanches in flowing granular matter. Nat. Commun. **7**, 10641 (2016). doi:10.1038/ncomms10641
25. Y. Ben-Zion, J.R. Rice, Slip patterns and earthquake populations along different classes of faults in elastic solids. J. Geophys. Res. **98**, 14109–14131 (1993)
26. Y. Ben-Zion, Collective behavior of earthquakes and faults: continuum-discrete transitions, progressive evolutionary changes and different dynamic regimes. Rev. Geophys. **46**, RG4006/1–70 (2008)
27. Y.Y. Kagan, Earthquake size distribution: power-law with exponent β=1/2? Tectonophysics **490**, 103–114 (2010)

28. S. Papanikolaou, F. Bohn, R.L. Sommer, G. Durin, S. Zapperi, J.P. Sethna, Universality beyond power laws and the average avalanche shape. Nat. Phys. **7**, 316 (2011)
29. S. Zapperi, C. Castellano, F. Colaiori, G. Durin, Signature of effective mass in crackling-noise asymmetry. Nat. Phys. **1**, 46 (2005)
30. A. Baldassarri, F. Colaiori, C. Castellano, Average shape of a fluctuation: universality in excursions of stochastic processes. Phys. Rev. Lett. **90**, 060601 (2003)
31. K.A. Dahmen, Nonlinear dynamics: universal clues in noisy skews. Nat. Phys. **1**, 13 (2005)
32. R. Maass, M. Wraith, J.T. Uhl, J.R. Greer, K.A. Dahmen, Slip statistics of dislocation avalanches under different loading modes. Phys. Rev. E **91**, 042403 (2015)
33. X. He, X. Ding, J. Sun, E.K.H. Salje, Parabolic temporal profiles of non-spanning avalanches and their importance for ferroic switching. Appl. Phys. Lett. **108**, 072904 (2016). doi:10.1063/1.4942387
34. B. Brinkman, M. LeBlanc, Y. Ben-Zion, J.T. Uhl, Karin A. Dahmen, Probing failure susceptibilities of earthquake faults using small-quake tidal correlations. Nature Commun. **6**, 6157 (2015). doi:10.1038/ncomms7157

http://www.springer.com/978-3-319-45610-2

Avalanches in Functional Materials and Geophysics

Salje, E.K.H.; Saxena, A.; Planes, A. (Eds.)
2017, XVII, 298 p. 171 illus., 80 illus. in color.,
Hardcover
ISBN: 978-3-319-45610-2